

# The isoscalar non-singlet axial form factor of the nucleon from lattice QCD

**Alessandro Barone,<sup>a,\*</sup> Dalibor Djukanovic,<sup>b,c</sup> Georg von Hippel,<sup>a</sup>  
Jonna Koponen,<sup>a</sup> Harvey B. Meyer,<sup>a,b</sup> Konstantin Ottnad<sup>a</sup> and Hartmut Wittig<sup>a,b</sup>**

<sup>a</sup>*PRISMA<sup>+</sup> Cluster of Excellence & Institut für Kernphysik, Johannes Gutenberg-Universität Mainz,  
D-55099 Mainz, Germany*

<sup>b</sup>*Helmholtz-Institut Mainz, Johannes Gutenberg-Universität Mainz, D-55099 Mainz, Germany*

<sup>c</sup>*GSI Helmholtzzentrum für Schwerionenforschung, Darmstadt (Germany)*

*E-mail:* [abarone@uni-mainz.de](mailto:abarone@uni-mainz.de)

We present our progress on the computation of the axial form factor of the nucleon with flavour structure  $u + d - 2s$  from lattice QCD. We employ a set of  $N_f = 2 + 1$  CLS ensembles with  $O(a)$ -improved Wilson fermions and the Lüscher-Weisz gauge action, with lattice spacings ranging from 0.05 fm to 0.086 fm and pion masses spanning between 130 MeV and 350 MeV. We employ multiple source-sink separations and use the summation method to suppress the contamination from excited states. We use a  $z$ -expansion on each ensemble to parametrize the  $Q^2$ -dependence of the form factor and simultaneously fit the available source-sink separations for all  $Q^2 \leq 0.7 \text{ GeV}^2$ . We outline our analysis of the stability of the fits varying the ansätze and different estimations of the covariance matrix and report on our strategy for a comprehensive determination of the physical form factor.

*The 41st International Symposium on Lattice Field Theory (LATTICE2024)  
28 July - 3 August 2024  
Liverpool, UK*

---

\*Speaker

## 1. Introduction

The axial form factors  $G_A(Q^2)$  of the nucleon plays a key role in understanding its (quasi-) elastic interactions with neutrinos. In particular, the isoscalar channel is sensitive to elastic scattering mediated by a  $Z$ , namely the strange axial form factor  $G_A^s(Q^2)$ , whereas the isovector channel  $G_A^{u-d}(Q^2)$  is sensitive to the  $W$  boson exchange. The strange form factor can be obtained combining the isoscalar singlet  $G_A^{u+d+s}(Q^2)$  and isoscalar octet  $G_A^{u+d-2s}(Q^2)$  contributions. Furthermore, the strange form factor provides information about the nucleon spin, which can be decomposed into contributions from the intrinsic quark spin, which is related to the axial charge  $g_A$ , the quark angular momentum and the gluon angular momentum [1, 2].

While the isovector contribution has recently received much attention from the community (see [3, 4] for a review), the isoscalar counterpart has not yet been addressed extensively [5]. However, a theoretical input for  $G_A^s(Q^2)$  is becoming timely, since experiments such as MicroBooNE [6, 7] are aiming to extract the strange form factor in the range  $Q^2[\text{GeV}^2] \in [0.08, 1]$ . In this work, we focus on the computation of the axial form factor in the non-singlet channel for an extended range of  $Q^2$ . We report preliminary results for the connected data  $u + d$  to illustrate the complete procedure and give a preview of the full  $u + d - 2s$  case on a few ensembles.

## 2. Lattice setup

The form factor appears in the parametrisation of the nucleon-nucleon matrix element with the isoscalar current insertion  $A_\mu^{u+d-2s} = \bar{u}\gamma_\mu\gamma_5 u + \bar{d}\gamma_\mu\gamma_5 d - 2\bar{s}\gamma_\mu\gamma_5 s$ , as

$$\langle N(p', s') | A_\mu^{u+d-2s} | N(p, s) \rangle = \bar{U}^{s'}(p') \left[ \gamma_\mu\gamma_5 G_A(Q^2) - \frac{Q_\mu}{2M_N} \gamma_5 G_P(Q^2) \right] U^s(p), \quad (1)$$

where  $U^s(p)$  is an isodoublet Dirac spinor with momentum  $p$  and spin  $s$ .

To address  $G_A$ , we calculate nucleon two- and three-point correlation functions starting from the nucleon interpolating operator  $\Psi^\alpha(x) = \epsilon_{abc} (\tilde{u}_a(x) C \gamma_5 \tilde{d}_b(x)) \tilde{u}_c^\alpha(x)$ , with  $\tilde{u}(x)$  and  $\tilde{d}(x)$  being the smeared up and down quark fields, respectively. In particular, for the three-point correlators we distinguish connected and disconnected contributions as

$$\begin{aligned} C_{3\text{pt},i}(\mathbf{q}, t, t_s) &= \sum_{\mathbf{x}, \mathbf{y}} e^{i\mathbf{q}\cdot\mathbf{y}} \Gamma_{\beta\alpha} \left\langle \bar{\Psi}^\alpha(\mathbf{x}, t_s) A_i^{u+d-2s}(\mathbf{y}, t) \Psi^\beta(0) \right\rangle \\ &= C_{3\text{pt},i}^{\text{conn}}(\mathbf{q}, t, t_s) + C_{3\text{pt},i}^{\text{disc}}(\mathbf{q}, t, t_s) \end{aligned} \quad (2)$$

with

$$C_{3\text{pt},i}^{\text{disc}}(\mathbf{q}, t, t_s) = \left\langle L_i(\mathbf{q}, t) C_2(\mathbf{p}', t_s) \right\rangle, \quad L_i(\mathbf{q}, t) = - \sum_{\mathbf{z}} e^{i\mathbf{q}\cdot\mathbf{z}} \text{Tr} \left[ D_q^{-1}(\mathbf{z}, \mathbf{z}) \gamma_i \gamma_5 \right], \quad (3)$$

where the connected part contains only  $u + d$ , and the strange quark  $s$  appears only in disconnected loops. We choose  $\mathbf{p}' = \mathbf{0}$ ,  $\mathbf{q} = \mathbf{p}' - \mathbf{p} = -\mathbf{p}$ , i.e. rest frame of the final state nucleon. We employ smeared quark fields and APE-smeared gauge fields in constructing  $\Psi^\alpha$ . For the multiplicative renormalisation factor of the non-singlet current we refer to [8], and we take the factors  $Z_A$  from [9]

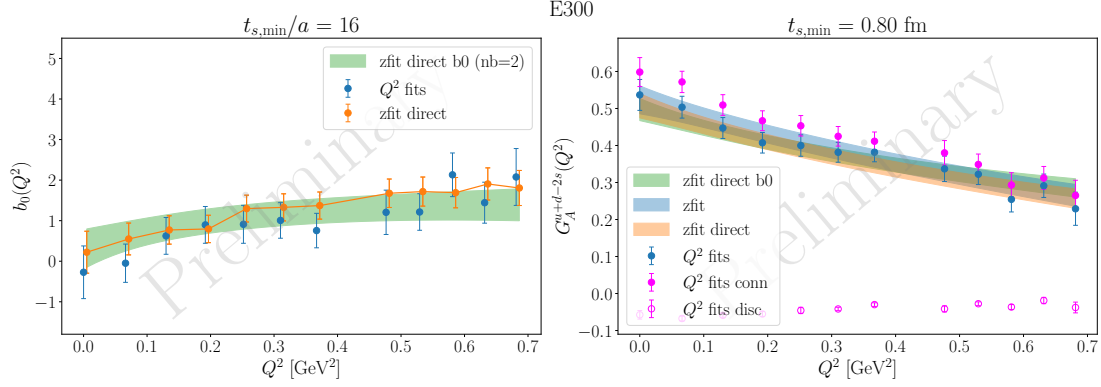


**Figure 1:** Comparison of different  $z$ -fit procedures for the ansatz in Eq. (7) for  $u + d - 2s$  data on E300. The blue points refer to the two-step procedure, and the orange points to the “direct” approach. The green bands complement the latter considering the case where  $b_0$  is also parametrised by a  $z$ -expansion at order  $n_b = 2$ . The magenta points show the contribution of the connected and disconnected data in the two-step procedure for illustration purposes.

and  $b_A$  from [10], neglecting the coefficient  $\tilde{b}_A$  and  $f_A$  (in the notation of [10]), which are assumed to be small since they parametrise sea-quark effects.

The axial form factor  $G_A$  is isolated considering the transverse component

$$C_{3\text{pt},i}^T(\mathbf{q}, t, t_s) = \epsilon^{ijk} q_j C_{3\text{pt},k}(\mathbf{q}, t, t_s) \propto (\mathbf{q} \times \boldsymbol{\gamma})_i \gamma_5 G_A(Q^2), \quad (4)$$

which is then projected into

$$C_{3\text{pt}}(\mathbf{q}, t, t_s) = \sum_i \frac{(\mathbf{q} \times \mathbf{s})_i}{|\mathbf{q} \times \mathbf{s}|^2} C_{3\text{pt},i}^T(\mathbf{q}, t, t_s), \quad \mathbf{s} = \mathbf{e}_3, \quad \Gamma = \frac{1}{2}(1 + \gamma_0)(1 + i\gamma_5\gamma_3). \quad (5)$$

The signal is improved considering only momenta  $|q_3| \leq \min(|q_1|, |q_2|)$ , after which we can build the ratio

$$R(\mathbf{q}, t, t_s) = \frac{C_{3\text{pt}}(\mathbf{q}, t, t_s)}{C_{2\text{pt}}(\mathbf{0}, t_s)} \sqrt{\frac{C_{2\text{pt}}(\mathbf{q}, t_s - t) C_{2\text{pt}}(\mathbf{0}, t) C_{2\text{pt}}(\mathbf{0}, t_s)}{C_{2\text{pt}}(\mathbf{0}, t_s - t) C_{2\text{pt}}(\mathbf{q}, t) C_{2\text{pt}}(\mathbf{q}, t_s)}}, \quad (6)$$

which is directly related to the effective form factor  $G_A^{\text{eff}}(Q^2)$  in the limit  $t_s - t \gg 0$ .

The calculations are performed employing a set of  $N_f = 2 + 1$  CLS ensembles [11] with  $O(a)$ -improved Wilson fermions [12, 13] and the Lüscher-Weisz gauge action [14], with lattice spacings ranging from 0.05 fm to 0.086 fm and pion masses ranging from 130 MeV to 350 MeV. We refer to [15] for the full details (see in particular Tab. I).

### 3. Analysis strategy

The analysis strategy follows and extends the one presented in [15]. We employ the summation method [16, 17]

$$S(\mathbf{q}, t_s) = a \sqrt{\frac{2E_q}{M_N + E_q}} \sum_{t=a}^{t_s-a} R(\mathbf{q}, t, t_s) \stackrel{t_s \gg 1}{\approx} b_0(Q^2) + t_s G_A(Q^2) + O(t_s e^{-\Delta t_s}), \quad (7)$$

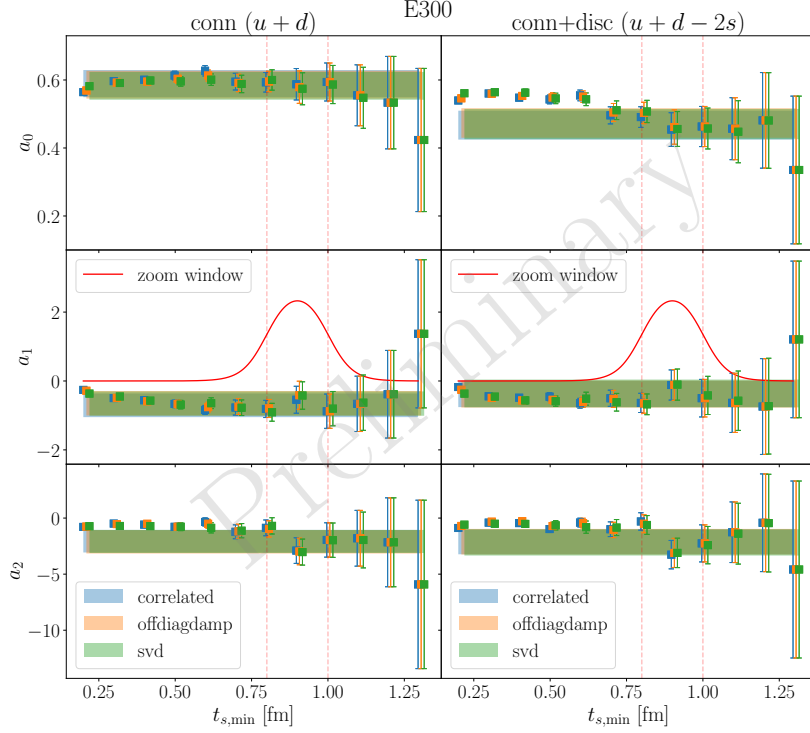


**Figure 2:** Window average on the coefficients  $a_0, a_1, a_2$  (rows) of the  $z$ -expansion in Eq. (8) as a function of the minimum source-sink separation  $t_{s,\min}$  on the ensemble E300 for the connected case (left) and the full octet case (right). The different colours refer to different approaches to regularise the covariance matrix, and the red curve is a zoom on the window function in Eq. (9). The vertical lines correspond to the choices of  $t_w^{\text{low}}$  and  $t_w^{\text{up}}$  and the horizontal bands indicate the final results of the window average on all points.

which allows us to extract the form factor  $G_A(Q^2)$  through a linear fit of the above expression in the source-sink separation  $t_s$ . We parametrise the form factor using the  $z$ -expansion at order  $n = 2$  as

$$G_A(Q^2) = \sum_{k=0}^n a_k z^k(Q^2), \quad z(Q^2) = \frac{\sqrt{t_{\text{cut}} + Q^2} - \sqrt{t_{\text{cut}}}}{\sqrt{t_{\text{cut}} + Q^2} + \sqrt{t_{\text{cut}}}}, \quad (8)$$

where we set  $t_{\text{cut}} = (4M_\pi)^2$  for all the ensembles and  $Q_{\text{max}}^2 = 0.7 \text{ GeV}^2$ . The typical two-step procedure consists in extracting  $G_A(Q^2)$  from a linear fit to Eq. (7) for all  $t_s$ , and then performing a  $z$ -fit over the selected points on the  $Q^2$  range to extract  $a_i$ ; instead, here we perform a single  $z$ -fit on all data including all  $t_s \in \{t_{s,\min}, \dots\}$  and  $Q^2 \in \{0, \dots, Q_{\text{max}}^2\}$  to extract directly the  $z$ -expansion coefficients on each ensemble. This allows us to smoothen the analysis strategy, providing a solid estimate of  $a_i$  for each  $t_{s,\min}$  with a single fit.

We compare these procedures in Fig. 1, considering both the case where  $b_0(Q^2)$  is treated as a fit parameter for each  $Q^2$  (orange and blue points) or the case where it is also parametrised with a  $z$ -expansion  $b_0(Q^2) = \sum_{k=0}^{n_b} d_k z^k(Q^2)$  at order  $n_b = 2$ . The plot shows that all approaches are compatible within errors.

The fits are performed starting from a minimum value of the source-sink separation  $t_{s,\min}$ , such that the coefficients  $a_i$  of the  $z$ -expansion depend on this choice. To obtain the final coefficients we

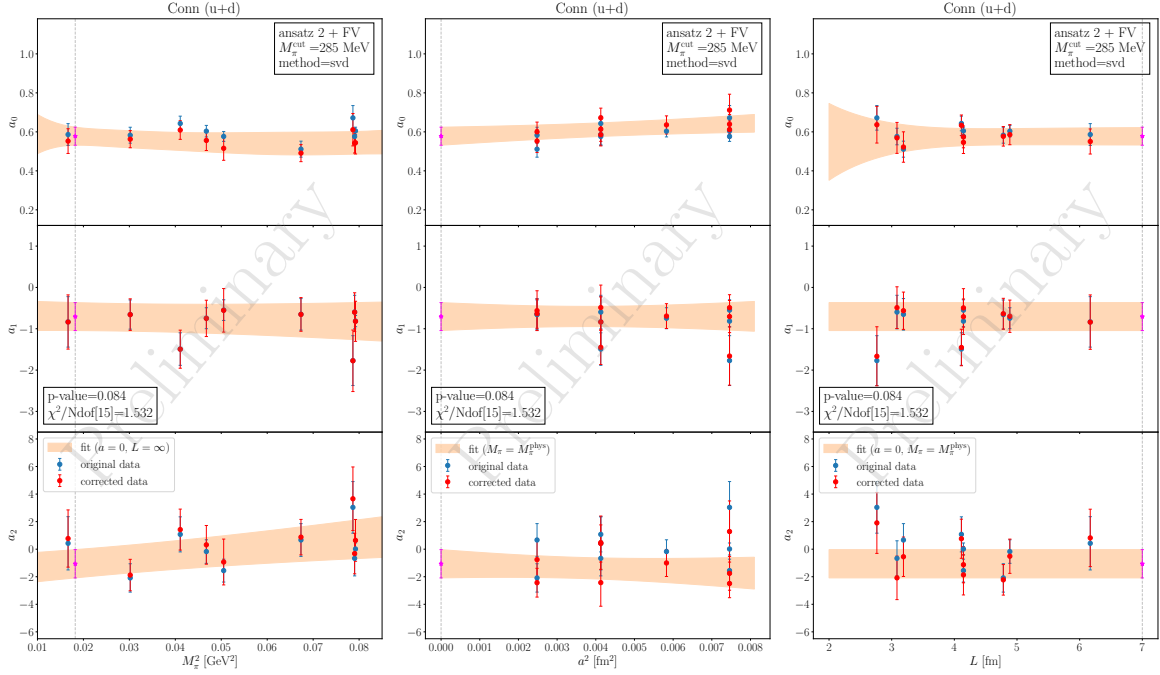


**Figure 3:** Example of chiral-continuum extrapolation for the  $u + d$  case with ansatz 2 and finite-volume effect with a cut  $M_\pi^{\text{cut}} = 285$  MeV, shown for all the three coefficients (rows) as a function of  $M_\pi^2$  (left),  $a^2$  (centre) and the spatial lattice size  $L$  (right). The blue points are the original data and the red points and band correspond to the corrected version for the continuum parameters as specified in the legend.

perform a weighted average over all these values assigning the weights according to the window function

$$W = \frac{1}{N_w} \left[ \tanh \left( \frac{t_s^{\text{min}} - t_w^{\text{low}}}{\Delta t_w} \right) - \tanh \left( \frac{t_s^{\text{min}} - t_w^{\text{up}}}{\Delta t_w} \right) \right], \quad (9)$$

where  $N_w$  is a normalisation factor and  $t_s^{\text{low}} = 0.8$  fm,  $t_s^{\text{up}} = 1$  fm,  $\Delta t_w = 0.08$  fm on each ensemble, in order to reduce the human bias in the procedure.

While the direct  $z$ -fit provides a simple solution to fitting simultaneously a large amount of data, it comes with the downside of dealing with a sizeable  $N \times N$  covariance matrix, with  $N = N_{Q^2} \times N_{t_s}$  being respectively the number of  $Q^2$  and source-sink separations  $t_s$  entering the fit. We therefore explore two different ways of regulating such a matrix. The first one consists in introducing a small damping  $\alpha \in [0.985, 1]$  on the off-diagonal elements [15]; the second relies on an svd cut to decrease the condition number of the matrix. We compare the methods in Fig. 2 against the unregulated matrix (“correlated”) to demonstrate that the estimation of the covariance is solid, as different regularisations provide negligible differences. We quote our final results using the svd approach.

#### 4. Preliminary results

In this section we highlight the final steps of the analysis on the connected data, namely the chiral-continuum extrapolation of the coefficients of the  $z$ -expansion and the model average, and

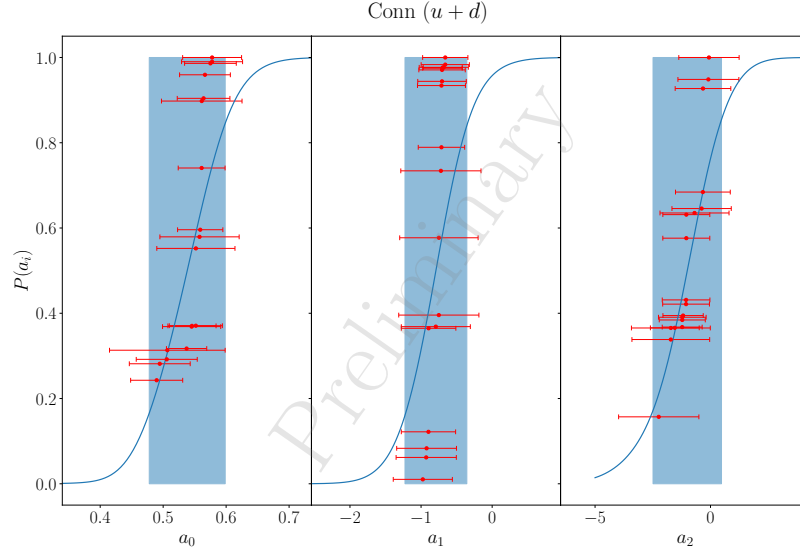


**Figure 4:** Model average through AIC for the  $u + d$  case. The red points correspond to the results of the fits entering the model average, and the blue line is the cumulative distribution in Eq. (12), with the vertical bands indicating the final results obtained from the 16th and 84th percentiles.

compare with preliminary results on the full dataset of two of our most chiral ensembles.

We consider three ansätze:

1. linear in  $M_\pi^2$  and  $a^2$  for each coefficient  $a_i$ ;
2. same as ansatz 1 with the addition of an  $M_\pi^3$  term and a log term for the axial charge  $a_0$ ;
3. same as ansatz 2 with the addition of  $M_\pi^3$  terms for  $a_1$  and  $a_2$ .

To account for finite-volume effects, we also consider all the previous ansätze with the correction term

$$\frac{M_\pi^2}{\sqrt{M_\pi L}} e^{-M_\pi L} \quad (10)$$

for  $a_0$ . We show an example of the chiral-continuum extrapolation of the connected data with ansatz 2 and finite-volume effects in Fig. 3, as a function of  $M_\pi^2$ ,  $a^2$  and the spatial lattice size  $L$ . The plot shows that the behaviour is quite flat for all the three variables, suggesting that the simple ansatz 1 would be enough to describe the data. In addition, finite-volume effects appear to be negligible.

We perform multiple fits with cuts in the pion mass,  $M_\pi^{\text{cut}} [\text{MeV}] = \{300, 285, 265\}$ , and cuts in the coarsest lattice spacing, while preserving the correlations among the three coefficients on each ensemble. We then obtain the final result through model average exploiting the version of the Akaike Information Criterion proposed in [18], i.e. assigning to each  $k$ -th fit the weight

$$w_k^{\text{AIC}} \propto e^{-\frac{1}{2}(\chi_k^2 + 2n_{\text{par},k} - n_{\text{data},k})}, \quad (11)$$

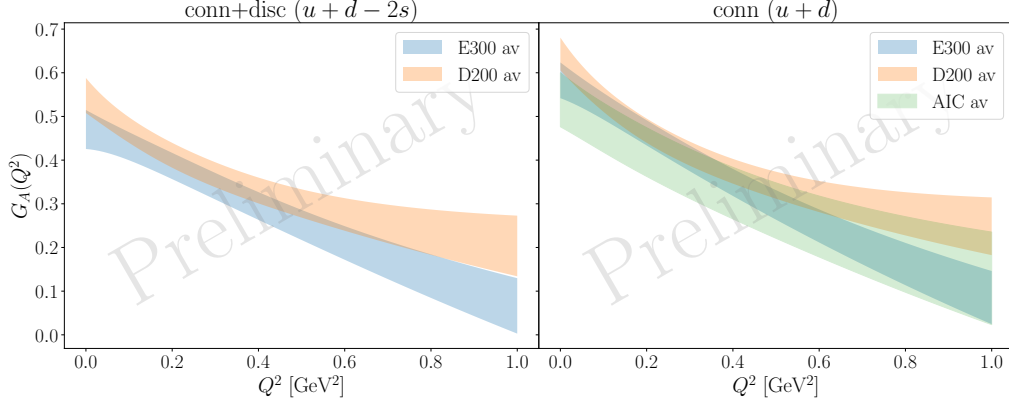


**Figure 5:** Final results on the isoscalar axial form factor  $G_A(Q^2)$  on the ensembles E300 and D200 after window average for both connected (right) and full case (left), compared with the final AIC average for the connected case only in green.

with  $n_{\text{par},k}$  being the number of parameters and  $n_{\text{data},k}$  the number of data points entering the fit, and obtaining the final results exploiting the 16th, 50th and 84th percentiles of the cumulative distributions

$$P(a_i) = \int_{-\infty}^{a_i} da'_i \sum_k w_k^{\text{AIC}} \mathcal{N}(a'_i; \langle a_i^{(k)} \rangle, \sigma_{a_i^{(k)}}^2) \quad (12)$$

obtained from a weighted sum of normal distributions centered on  $\langle a_i^{(k)} \rangle$  and variance  $\sigma_{a_i^{(k)}}^2$  for each  $z$ -expansion coefficient  $a_i$  and fit  $k$ . The procedure is shown in Fig. 4. The correlations are taken into account repeating the same procedure for the cumulative distributions  $P(a_i a_j)$  and extracting them from the standard relations between the variances  $\text{var}[a_i a_j]$ ,  $\text{var}[a_i]$  and  $\text{var}[a_j]$ .

We illustrate the preliminary results in Fig. 5, where we compare the connected  $u+d$  contribution after model average to two of the most chiral ensembles E300 and D200 (right); the full  $u + d - 2s$  from factor is displayed on the left for these two ensembles. We can see that for the connected case the two ensembles already seem to provide a good description of the physical case. The disconnected pieces contribute mainly at low  $Q^2$  (cf. Fig. 1) yielding a shift of the form factor mainly in that region. While this preliminary evaluation is obtained only on two ensembles, i.e without accounting for lattice artifacts, these provide a value of the axial charge compatible with  $g_A^{u+d-2s} = 0.46(5)$  obtained using the Cloudy Bag model [19], as well as the most recent result from the ETM collaboration  $g_A^{u+d-2s} = 0.490(20)$  [20].

## 5. Outlook and conclusions

In this proceedings contribution we have outlined our analysis strategy for the non-singlet isoscalar axial form factor, reporting some preliminary results for both the connected and the full case on a few ensembles. In particular, we exploit the summation method combined with a direct  $z$ -expansion to order  $n = 2$ , comparing various techniques to regulate the large covariance matrix, namely off-diagonal damping and svd cuts. The  $z$ -expansion coefficients are obtained from each

ensemble through a window average of the minimum source-sink separations - which have been kept in physical units across all ensembles in order to reduce the human bias - and then extrapolated to the chiral-continuum limit with different ansätze and cuts both in pion mass and lattice spacing. The final result is then obtained through a model average.

To complete the analysis, several steps have to be taken. First of all, we will include the disconnected contributions on all ensembles to extend the analysis to the full  $u + d - 2s$  case. We plan to explore more fit ansätze (e.g. dipole) to cross-check the quality of our data and the performance of our analysis. Once complete, this study will provide a first physical result for the isoscalar octet of the nucleon axial form factor in a large  $Q^2$  range accessible by experiments. Furthermore, it will provide a first step into the flavour decomposition of the form factor, for which we require a similar analysis for the singlet  $u + d + s$  contribution.

## Acknowledgments

This work was supported in part by the European Research Council (ERC) under the European Union’s Horizon 2020 research and innovation program through Grant Agreement No. 771971-SIMDAMA and by the Deutsche Forschungsgemeinschaft (DFG) through the Collaborative Research Center 1660 “Hadrons and Nuclei as Discovery Tools”, under grant HI 2048/1-3 (Project No. 399400745) and in the Cluster of Excellence “Precision Physics, Fundamental Interactions and Structure of Matter” (PRISMA+ EXC 2118/1) funded by the DFG within the German Excellence strategy (Project ID 39083149). Calculations for this project were partly performed on the HPC clusters “Clover” and “HIMster2” at the Helmholtz Institute Mainz, and “Mogon 2” at Johannes Gutenberg-Universität Mainz. The authors gratefully acknowledge the Gauss Centre for Supercomputing e.V. ([www.gauss-centre.eu](http://www.gauss-centre.eu)) for funding this project by providing computing time on the GCS Supercomputer systems JUQUEEN and JUWELS at Jülich Supercomputing Centre (JSC) via grants HMZ21, HMZ23 and HMZ36 (the latter through the John von Neumann Institute for Computing (NIC)), as well as on the GCS Supercomputer HAZELHEN at Höchstleistungsrechenzentrum Stuttgart ([www.hlr.de](http://www.hlr.de)) under project GCS-HQCD.

Our programs use the QDP++ library [21] and deflated SAP+GCR solver from the openQCD package [22], while the contractions have been explicitly checked using [23]. We are grateful to our colleagues in the CLS initiative for sharing the gauge field configurations on which this work is based.

## References

- [1] X.-D. Ji, *Gauge-Invariant Decomposition of Nucleon Spin*, *Phys. Rev. Lett.* **78** (1997) 610 [[hep-ph/9603249](#)].
- [2] COMPASS collaboration, *The Deuteron Spin-dependent Structure Function  $g_1(d)$  and its First Moment*, *Phys. Lett. B* **647** (2007) 8 [[hep-ex/0609038](#)].
- [3] A.S. Meyer, M. Betancourt, R. Gran and R.J. Hill, *Deuterium target data for precision neutrino-nucleus cross sections*, *Phys. Rev. D* **93** (2016) 113015 [[1603.03048](#)].



- [4] A.S. Meyer, A. Walker-Loud and C. Wilkinson, *Status of Lattice QCD Determination of Nucleon Form Factors and their Relevance for the Few-GeV Neutrino Program*, *Ann. Rev. Nucl. Part. Sci.* **72** (2022) 205 [[2201.01839](#)].
- [5] C. Alexandrou, S. Bacchio, M. Constantinou, K. Hadjiyiannakou, K. Jansen and G. Koutsou, *Quark flavor decomposition of the nucleon axial form factors*, *Phys. Rev. D* **104** (2021) 074503 [[2106.13468](#)].
- [6] MICROBooNE collaboration, *Improving Dark Matter Searches by Measuring the Nucleon Axial Form Factor: Perspectives from MicroBooNE*, *Phys. Procedia* **61** (2015) 495 [[1406.5204](#)].
- [7] K.S. Kim, K.-S. Choi, M.-K. Cheoun, W.Y. So and H. Moon, *Role of axial mass and strange axial form factor from various target nuclei in neutrino-nucleus scattering*, *Phys. Rev. C* **100** (2019) 034604.
- [8] T. Bhattacharya, R. Gupta, W. Lee, S.R. Sharpe and J.M.S. Wu, *Improved bilinears in lattice QCD with non-degenerate quarks*, *Phys. Rev. D* **73** (2006) 034504 [[hep-lat/0511014](#)].
- [9] M. Dalla Brida, T. Korzec, S. Sint and P. Vilaseca, *High precision renormalization of the flavour non-singlet Noether currents in lattice QCD with Wilson quarks*, *Eur. Phys. J. C* **79** (2019) 23 [[1808.09236](#)].
- [10] P. Korcyl and G.S. Bali, *Non-perturbative determination of improvement coefficients using coordinate space correlators in  $N_f = 2 + 1$  lattice QCD*, *Phys. Rev. D* **95** (2017) 014505 [[1607.07090](#)].
- [11] M. Bruno et al., *Simulation of QCD with  $N_f = 2 + 1$  flavors of non-perturbatively improved Wilson fermions*, *JHEP* **02** (2015) 043 [[1411.3982](#)].
- [12] B. Sheikholeslami and R. Wohlert, *Improved Continuum Limit Lattice Action for QCD with Wilson Fermions*, *Nucl. Phys. B* **259** (1985) 572.
- [13] J. Bulava and S. Schaefer, *Improvement of  $N_f = 3$  lattice QCD with Wilson fermions and tree-level improved gauge action*, *Nucl. Phys. B* **874** (2013) 188 [[1304.7093](#)].
- [14] M. Luscher and P. Weisz, *On-shell improved lattice gauge theories*, *Commun. Math. Phys.* **98** (1985) 433.
- [15] D. Djukanovic, G. von Hippel, J. Koponen, H.B. Meyer, K. Ottnad, T. Schulz et al., *Isovector axial form factor of the nucleon from lattice QCD*, *Phys. Rev. D* **106** (2022) 074503 [[2207.03440](#)].
- [16] L. Maiani, G. Martinelli, M.L. Paciello and B. Taglienti, *Scalar Densities and Baryon Mass Differences in Lattice QCD With Wilson Fermions*, *Nucl. Phys. B* **293** (1987) 420.
- [17] S. Capitani, M. Della Morte, G. von Hippel, B. Jager, A. Juttner, B. Knippschild et al., *The nucleon axial charge from lattice QCD with controlled errors*, *Phys. Rev. D* **86** (2012) 074502 [[1205.0180](#)].

- [18] S. Borsanyi et al., *Leading hadronic contribution to the muon magnetic moment from lattice QCD*, *Nature* **593** (2021) 51 [2002.12347].
- [19] S.D. Bass and A.W. Thomas, *The nucleon's octet axial-charge  $g_A^{(8)}$  with chiral corrections*, *Phys. Lett. B* **684** (2010) 216 [0912.1765].
- [20] C. Alexandrou, S. Bacchio, J. Finkenrath, C. Iona, G. Koutsou, Y. Li et al., *Nucleon charges and  $\sigma$ -terms in lattice QCD*, [2412.01535](#).
- [21] SciDAC, LHPC, UKQCD collaboration, *The Chroma software system for lattice QCD*, *Nucl. Phys. B Proc. Suppl.* **140** (2005) 832 [[hep-lat/0409003](#)].
- [22] M. Luscher and S. Schaefer, *Lattice QCD with open boundary conditions and twisted-mass reweighting*, *Comput. Phys. Commun.* **184** (2013) 519 [1206.2809].
- [23] D. Djukanovic, *Quark Contraction Tool — QCT*, *Comput. Phys. Commun.* **247** (2020) 106950 [1603.01576].